Coupled Heterogeneous Nanowire–Nanoplate Planar Transistor Sensors for Giant (>10 V/pH) Nernst Response

Jonghyun Go,[†,*] Pradeep R. Nair,[†,¶] Bobby Reddy, Jr.,[‡,∥] Brian Dorvel,[§,∥] Rashid Bashir,[‡,⊥,∥] and Muhammad A. Alam[†,*]

[†]School of Electrical and Computer Engineering, Purdue University, West Lafayette, Indiana, United States, [‡]Department of Electrical and Computer Engineering, [§]Department of Biophysics, [⊥]Department of Bioengineering and [∥]Micro and Nanotechnology Laboratory, University of Illinois at Urbana–Champaign, Urbana, Illinois, United States, and [¶]Department of Electrical Engineering, Indian Institute of Technology Bombay, India

ABSTRACT

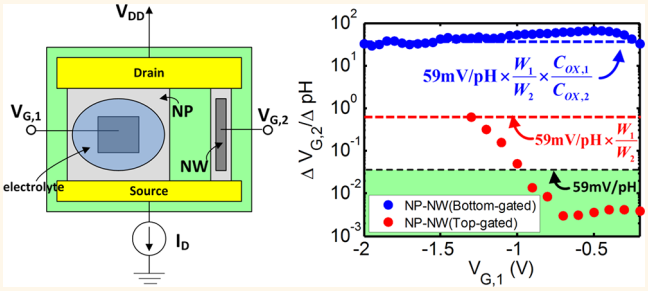

We offer a comprehensive theory of pH response of a coupled ISFET sensor to show that the maximum achievable response is given by $\Delta V/\Delta\text{pH} = 59\text{ mV/pH} \times \alpha$, where 59 mV/pH is the intrinsic Nernst response and α an amplification factor that depends on the geometrical and electrical properties of the sensor and transducer nodes. While the *intrinsic* Nernst response of an electrolyte/site-binding interface is fundamental and immutable, we show that by using channels of different materials, areas, and bias conditions, the *extrinsic* sensor response can be increased dramatically beyond the Nernst limit. We validate the theory by measuring the pH response of a Si nanowire–nanoplate transistor pair that achieves >10 V/pH response and show the potential of the scheme to achieve (asymptotically) the theoretical lower limit of signal-to-noise ratio for a given configuration. We suggest the possibility of an even larger pH response based on recent trends in heterogeneous integration on the Si platform.

KEYWORDS: pH sensor · field effect transistor · Nernst limit · nanowire–nanoplate · limit of biosensors

The search for a miniaturized, highly integrated, and lower cost replacement of the Beckman pH meter[1] dates back to the 1970s, when Bergveld proposed the CMOS-compatible concept of ion-sensitive field effect transistors[2] (ISFETs, Figure 1a). Modern variants of ISFETs, based on silicon nanowires (Si-NWs)[3] and carbon nanotubes (CNTs),[4] offer a novel form factor, prospects of innovative integration, and broader applications, but the sensitivity of all ISFETs is still defined by 59 mV/pH, the Nernst limit associated with an electrolyte and a site-binding surface. Many modern applications of ISFETs, such as the label-free detection of biomolecules in human genome sequencing,[5] however, require the ability to detect just a few hundred protons ($\Delta\text{pH} \approx 0.02$) in rapid flux (millisecond response). For these applications, the ability to amplify the Nernst signal can simplify the design and increase throughput.

A recent trend for such amplification has been based on double-gate silicon-on-insulator FET (DGFET), and a "super"-Nernst response of ~1 V/pH has been demonstrated.[6−9] As we will discuss below, the need to use a high fluid-gate bias, the poorer quality of the bottom oxide, and the high cost of a silicon-on-insulator (SOI) wafer suggest opportunities to develop alternative techniques. In this paper, we offer such an alternative based on a highly integrated Si nanoplate (NP)–nanowire (NW) transistor pair that is compatible with planar Si processing technology; see Figure 1c. In this configuration, the nanoplate acts as the pH sensor node biased through the fluid gate, while the transducer node, defined by the NW, can be biased either through the top gate (top-gated NW) or the bottom gate (bottom-gated NW), as shown in Figure 1d. Although term "nanoplate" has traditionally been used to describe objects with ~100 nm dimensions, here we use the term to describe a transistor that is ~100 nm thick (and a few μm wide) to emphasize its

* Address correspondence to jonghyungo@ieee.org, alam@purdue.edu.

Received for review February 27, 2012 and accepted June 13, 2012.

Published online June 13, 2012
10.1021/nn300874w

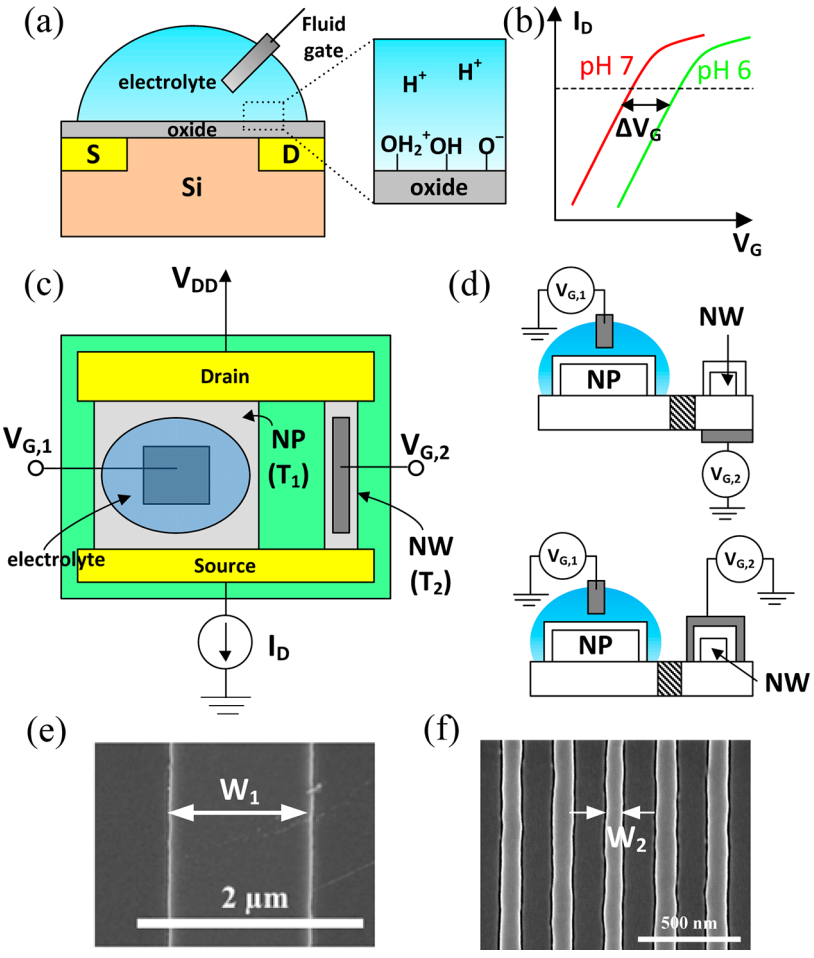

Figure 1. (a) Schematic diagram of a standard ISFET pH sensor. The surface groups (OH) react with protons (H^+) in electrolyte, and the reaction products (OH_2^+ and O^-) create a net surface charge. (b) Changes in the pH of the electrolyte are reflected in the change of surface charge and eventually changes in channel current (I_D) from source (S) to drain (D). The change in fluid-gate bias (ΔV_G) required to restore I_D to the original value defines the pH sensitivity of the ISFET. (c) Top view of a coupled nanoplate (NP)−nanowire (NW) pH sensor. NP is always biased by the fluid gate, but the NW can be biased *via* the top or bottom gate, illustrated as schematics in (d). (e, f) SEM images of a nanoplate (top view) and five nanowires (top view). Only one of the NWs is used as T_2 for the sensor scheme proposed.

pairing with a NW transistor. The configuration obviates the need for high fluid bias for the NP pH-sensor node and yet achieves an amplified Nernst response of ~1 V/pH with a top-gated NW and (even superior) >10 V/pH with a bottom-gated NW. Finally, we conclude by emphasizing the theoretical possibility of an even higher pH response with transistors of different materials integrated onto a common substrate (In Figure 1, both NW and NP are made of Si.) The maximum sensitivity achievable by the scheme is defined by the fundamental trade-off between dynamic range and sensitivity, and practical requirements of the transistor technology.

Operation of Single- and Double-Gated ISFETs. A classical ISFET pH sensor involves a simple modification of the standard metal oxide field effect transistor (MOSFET) with the poly-Si gate (on top of the gate oxide) replaced by an electrolyte and a fluid gate, as shown in Figure 1a. Instead of using a poly-Si gate to control the channel current in Si, in the ISFET the fluid gate affects the source (S) to drain (D) channel current I_D *via* an electrolyte. Any shift in pH of the electrolyte changes the surface charge at the electrolyte−oxide interface through the site-binding process. As shown in Figure 1b, that ISFET detects pH shifts in the electrolyte by monitoring changes in the Si channel current due to charge modulation of the surface group at the electrolyte−oxide interface.[10] The pH sensitivity is obtained by measuring the shift of the fluid-gate voltage (ΔV_G) at a given amount of pH changes in constant current operation.

The pH sensitivity of an ISFET can be understood simply as follows (see ref 10 for a detailed analysis): The amphoteric OH groups at the gate oxide/buffer undergo protonation/deprotonation of the interface as a function of surface proton density, $[H^+]_S$. Assuming Boltzmann distribution for ions in the buffer solution, we have

$$[H^+]_S = [H^+]_B e^{-q(\psi_0 - V_G)/k_B T} = e^{-2.303\mathrm{pH} - q(\psi_0 - V_G)/k_B T} \quad (1)$$

where $[H^+]_B$ is the bulk proton density, $pH = -\log_{10}[H^+]_B$, ψ_0 is the oxide/buffer interface potential, k_B is the Boltzmann constant, and T is the temperature. Accordingly, any change in buffer pH manifests as an effective change in surface potential (or an effective change in applied bias for constant current operation) as $\Delta V_G \approx 2.303(k_BT/q)\Delta pH$. Hence the maximum pH sensitivity, known as the Nernst limit, is $\Delta V_G/\Delta pH$ = 59 mV/pH at room temperature. In practice, the sensitivity is always less than the intrinsic Nernst limit (associated with the electrolyte/oxide interface) due to the high electrolyte screening, protonation affinity of the sensor surface, and, most importantly, the finite semiconductor capacitance of an ISFET.[10]

Recently many experimental[6−8] and theoretical[9] works suggest that this response can be "amplified" through innovative device geometries; in fact, a super-Nernst sensitivity of ~1 V/pH can be achieved by using the double-gate SOI structures. There are two gates (top and bottom one) in a DGFET sensor. The key idea is to restore the change in I_D due to pH change not by the fluid gate (as in ISFET), but rather through the bottom gate. The conductance change at the top surface of the channel (due to pH shift) is compensated by the change in conductance at the bottom surface to maintain constant current operation. The corresponding pH sensitivity of a DGFET sensor is

$$\Delta V_G^{DGFET}/\Delta pH = (59\ mV/pH)\left(\frac{C_{tox}}{C_{box}}\right)\alpha_{SN} \quad (2)$$

where C_{tox} and C_{box} are the top and bottom gate oxide capacitance, so that the amplification factor $\alpha = (C_{tox}/C_{box})\alpha_{SN} \gg 1$. For DGFET sensors, the bias and geometry dependent factor $\alpha_{SN} \leq 1$, as discussed below. Note that the intrinsic Nernst limit (59 mV/pH), associated with the electrolyte and site-binding layer, is fundamental and cannot be changed by new device configurations (ISFET or DGFET) or novel transducers. The amplified extrinsic Nernst response, however, simplifies detection and improves practical signal-to-noise ratio (SNR).

For maximum sensitivity ($\alpha_{SN} \rightarrow 1$) of a DGFET sensor (eq 2), *the top channel of the device must be biased in inversion through the fluid gate*. Biasing the fluid gate at high voltage is challenging because (i) large fluidic bias may increase gate leakage and reduce device lifetime[11] and (ii) if the bias exceeds the formal potential of the electrode, the Butler−Volmer reaction[12] at the fluidic electrode may make the effective potential at the sensor surface undefined. Moreover, a shared bottom gate electrode of the DGFET technology makes it difficult to integrate multiple, individually accessible sensors within a common platform, as required in applications such as ref 4. Finally, applying too high a bias on the poorer quality bottom oxide may lead to hysteresis and unstable device operation. Hence, a super-Nernst sensor that does not require high fluid bias, is not constrained by the geometric/material features of the DGFET, and can be integrated better with the traditional planar technology is desirable.

Proposed Giant-Nernst (GN) Scheme. Consider an *accumulation-mode* NP−NW transistor pair, shown in Figure 1c. Here, the NP FET acts as a sensor transistor T_1 and is exposed to the buffer solution for pH sensing, while the NW FET T_2 acts as a transducer and is isolated from the buffer. Since the transistors are compatible with planar top-down technology and are processed simultaneously, the process is simple and no *additional* masks are necessary. Details of the process steps and standard protocols for pH measurement are discussed in the Method section.

For the accumulation-mode devices, the drain current modulation in T_2 is given as

$$\Delta I_{D,2} = \mu_2 C_{OX,2}(W/L)_2 V_{DS,2}\Delta V_{G,2} \quad (3)$$

where μ_2 is the channel mobility, $C_{OX,2}$ is the gate oxide capacitance, W and L are the channel width and length, $V_{DS,2}$ is the drain bias, and $\Delta V_{G,2}$ is the gate bias modulation. Since T_1 and T_2 are in the accumulation regime, the band bending at the channel surface is very small. Hence the current modulation of T_1 due to any *pH-induced* modulation of top-oxide/buffer interface potential is given by $\Delta I_{D,1} = \mu_1 C_{OX,1}(W/L)_1 V_{DS,1}\Delta V_{G,1}$ (note that $\Delta V_{G,1}$ is limited by the Nernst response). The proposed scheme requires that the bias of T_2 should be adjusted to counterbalance the conductance modulation of T_1, so that

$$\frac{\Delta V_{G,2}}{\Delta V_{G,1}} = \left(\frac{\mu_1}{\mu_2}\frac{(W/L)_1}{(W/L)_2}\frac{V_{DS,1}}{V_{DS,2}}\right)\frac{C_{OX,1}}{C_{OX,2}} = \alpha_{GN}\frac{C_{OX,1}}{C_{OX,2}} \quad (4)$$

Equation 4 suggests that the GN scheme can achieve significant amplification over DGFET sensors (*i.e.*, $\alpha_{GN} \gg \alpha_{SN}$) by (i) *scaling of device dimension*, so that W/L of T_1 far exceeds that of T_2 (and hence the use of a NP and NW transistor couple). (ii) *Mobility scaling*, so that T_1 has higher mobility than T_2. This can be achieved by using a NMOS/PMOS pair for T_1/T_2 or by using different channel materials. (iii) *Oxide thickness scaling*. This option is similar to the DGFETs. For maximum amplification, $C_{OX,1} \gg C_{OX,2}$. This is achieved through oxide thickness scaling in a dual oxide process or by using higher-k dielectrics for T_1 compared to T_2 or a combination thereof. (iv) *Bias scaling*, so that V_{DS} of T_2 is smaller than that of T_1. This option of bias scaling provides a postprocess, point-of-care option to tune the sensor performance. Since the geometry of DGFET precludes the use of device, bias, and mobility scaling, the response is typically limited to ~1 V/pH.

RESULTS AND DISCUSSIONS

Figure 2 demonstrates the experimental validation of the giant-Nernst scheme, with the maximum GN response of >10 V/pH. Let us consider two different

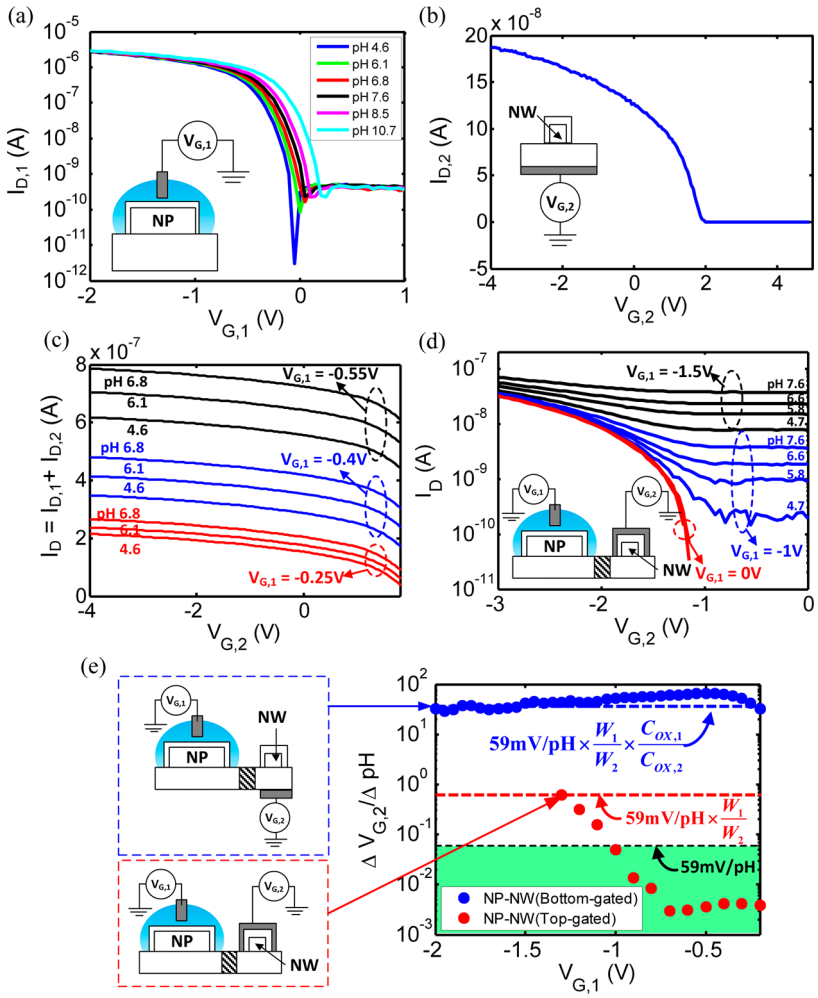

Figure 2. (a, b) Measured transfer characteristics of a nanoplate (serves as T_1) and bottom-gated nanowire (T_2), respectively. (c) Transfer characteristics of combined response of (a) and (b)—NP coupled with *bottom*-gated NW—plotted as a function of $V_{G,2}$. (d) Transfer characteristics of combined currents of a pair of NP and top-gated NW sensor with varying pH and $V_{G,1}$. (e) Measured pH sensitivity (circles) of coupled NP−NW sensors depending on NW bias configurations: bottom gate (blue dots, extracted from (c)) and top gate (red dots, extracted from (d)) sweep. The dashed blue/red lines indicate the corresponding theoretical estimates dictated by eq 4. The green region represents the classical sensitivity regime below the Nernst limit (59 mV/pH, dashed black line).

biasing configurations for the NW (T_2) illustrated in Figure 1d and compare their performances. In the first configuration, the nanowire T_2 is operated through the bottom gate (BG) and in the second one, through its top gate (TG); T_1 is always biased *via* the fluid gate.

To understand the overall response of the first configuration (bottom gate operation of T_2), we characterize the T_1−T_2 responses independently (Figure 2a and b). The pH sensitivity of a stand-alone nanoplate (T_1) is obtained by the measuring transfer characteristics ($I_{D,1}$ *vs* $V_{G,1}$) of a nanowire in solution for various pH values, as shown in Figure 2a. The responses are stable and repeatable over many hours of operation. We find that the stand-alone response of T_1 is 46 mV/pH, below the Nernst limit, as expected. For the GN amplification, T_1−T_2 coupling is essential, as predicted by eq 4. Figure 2b shows the isolated transfer characteristics ($I_{D,2}$ *vs* $V_{G,2}$) of the nanowire (T_2) measured in dry air with bottom gate operation.

Recalling the current change in T_1 ($\Delta I_{D,1}$) needs to be compensated by T_2 ($\Delta I_{D,2} = -\Delta I_{D,1}$), we obtain the "combined" transfer characteristics (I_D *vs* $V_{G,2}$ shown in Figure 2c), where the total current (I_D) is the sum of individual currents of T_1 ($I_{D,1}$) and now top-gated T_2 ($I_{D,2}$). Figure 2c shows the combined current *vs* the NW gate bias ($V_{G,2}$) with different $V_{G,1}$ and pH. Since the current change in T_1 needs to be compensated by T_2 (*i.e.*, $\Delta I_{D,1} + \Delta I_{D,2} = 0$ or $I_D = I_{D,1} + I_{D,2}$ is fixed), the NW gate bias $V_{G,2}$ needs to be shifted *vs* pH changes (ΔpH) at the constant current level of I_D *vs* $V_{G,2}$ in Figure 2c. For each $V_{G,1}$, we measure the shift of curves ($\Delta V_{G,2}$) at a constant current level. This measured sensitivity ($\Delta V_{G,2}$ /ΔpH) of the first configuration is shown in Figure 2e as blue dots. Since T_2 is operated *via* bottom gate and the channel lengths of T_1 and T_2 are the same ($L_1 = L_2$), the theoretical estimate of α_{GN} equals $(W/L)_1/(W/L)_2 \times (C_{OX,1}/C_{OX,2}) = (W_1/W_2) \times (EOT_{OX,2}/EOT_{OX,1})$ = (2 μm/50 nm) × (145 nm/7.3 nm) ≈ 794,

so the sensitivity is 46 mV/pH × 794 ≈ 36 V/pH, shown as the dashed blue line in Figure 2e, which is consistent with our measurement. This NP−NW sensitivity is significantly better than that of DGFET sensors (*i.e.*, $\alpha_{GN} \gg \alpha_{SN}$). This amplification reflects the fact that the current level of T_1 (Figure 2a) is 1−2 orders of magnitude higher than that of T_2 (Figure 2b) since the nanoplate (T_1) FET has a much higher *W/L* ratio compared to that of the nanowire (T_2) FET, specifically, $(W/L)_1 = 40 \times (W/L)_2$ for these particular devices. Note that it is not possible to obtain such high gain from DGFET sensors reported in the literature, because the oxide area, mobility, and drain bias of the sensor and transducer channels are coupled by a common substrate of DGFET, so that $\alpha_{SN} \approx 1$.

To measure the pH sensitivity in the second configuration of NW biasing (top gate operation of T_2, sensitivity shown as red dots in Figure 2e), we also measure "combined" transfer characteristics (I_D *vs* $V_{G,2}$ shown in Figure 2d) of a nanoplate and a top-gated nanowire. We follow the same procedure to extract the corresponding pH sensitivity as we did in the first configuration (with a bottom-gated nanowire). The red dots in Figure 2e show the pH sensitivity ($\Delta V_{G,2}$ / ΔpH) measured in T_2 as a function of NP fluid-gate bias ($V_{G,1}$). Since both T_1 and T_2 are biased *via* the top gate and have the same top oxide dimension, the sensitivity amplification is achieved by different *W/L* ratios. The effective transistor width of the NW sensor is $W_2^{eff} = W_2 + 2H_2 \approx 3W_2$, because the height of the nanowire (H_2) is similar to W_2 and the gate bias couples to all three surfaces electrostatically. The estimated sensitivity of 46 mV/pH × $(W_1/W_2^{eff}) \approx 0.613$ V/pH, shown as dashed red lines in Figure 2e, matches well with the experimental data in the accumulation regime. This result implies that the amplification comparable to DGFET can be easily achieved with conventional top-gated MOSFETs with proper design of the device geometries. Although the bottom-gated NW (blue dots, Figure 2e) gives a higher sensitivity compared to the top-gated NW configuration (red dots, Figure 2e) due to its thicker (bottom) oxide, in practice one cannot scale the bottom oxide arbitrarily without introducing excessive defects that lead to device instability and hysteresis. Also, the availability of a top contact simplifies the interconnection in a massively parallel circuit. Therefore, there may be many practical reasons to prefer the top-gated NW configuration for realistic device application.

Equation 4 suggests that the sensor response could *potentially* be further improved if the NP and NW sensors are made of different channel materials, so that their mobility asymmetry ($\mu_1/\mu_2 \gg 1$) can be used to amplify the sensor response. To estimate the possible gain in sensitivity by combing transistors of different materials, we first measure the transfer characteristics of a set of Si n-MOSFET devices, which would serve as the transducer node, T_2. Next, we extract the slopes of pH responses ($\Delta I_D/\Delta$pH) of devices with different channel materials[13−15] reported in the literature, each of which may potentially serve as the sensor node, T_1. Finally, we calculate the combined pH sensitivity of these heterogeneous T_1−T_2 pairs. Figure 3 compares the responses so obtained with those from DGFET and ISFETs sensors reported in the literature. As expected, regardless of the material characteristics or device dimensions, all the data from the literature based on DGFET and ISFET sensors (black symbols) lie below $\alpha_{SN} = 1$ line (the solid black line). In DGFET sensors,[6−8] a pH response of ~1 V/pH can be achieved. For the proposed GN scheme based on the T_1−T_2 pair, the corresponding pH sensitivity far exceeds the DGFET response ($\alpha_{GN} \gg 1$), especially with high-mobility devices (such as GaN, AlGaN) serving as T_1, and one can achieve even higher sensitivity (up to 100 V/pH regime) by pairing planar FETs with different materials and dimensions into a single sensing entity. Equation 4 therefore defines the fundamental upper limit of pH sensing for NW−NP based sensors. In practice, this upper limit may not be achieved due to fundamental and practical issues, as discussed in the next section.

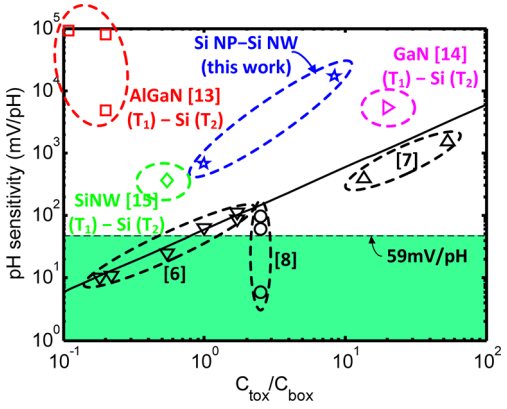

Figure 3. *Simulated* pH sensitivity of the GN scheme with various types of sensing devices (T_1 in Figure 1c) in the literature: AlGaN[13] (□)-, GaN[14] (▷)-, and SiNW[15] (◇)-based ISFETs. Here a Si n-MOSFET serves as T_2. The remaining (black) symbols indicate the experimental data from several DGFET sensors in the literature.[6−8] The solid black line represents the theoretical limit of the DGFET sensors, given by eq 2.

Considerations of Dynamic Range, SNR, and Minimum pH Resolution. In contrast to an ISFET pH sensor showing a wide dynamic range of pH sensing,[16] the high sensitivity of the GN scheme is realized at the expense of reduced dynamic range (analogous to the gain-bandwidth product of a traditional transistor). For many applications in healthcare, where the dynamic range of interest is small (7.35−7.45 for human blood pH; ΔpH ≈ 0.02 for ref 4), the trade-off of higher sensitivity for reduced dynamic range is fully justified. However, excessive gain would require repeated changing of the dc bias to cover the pH range of interest, which is cumbersome and counterproductive. In addition,

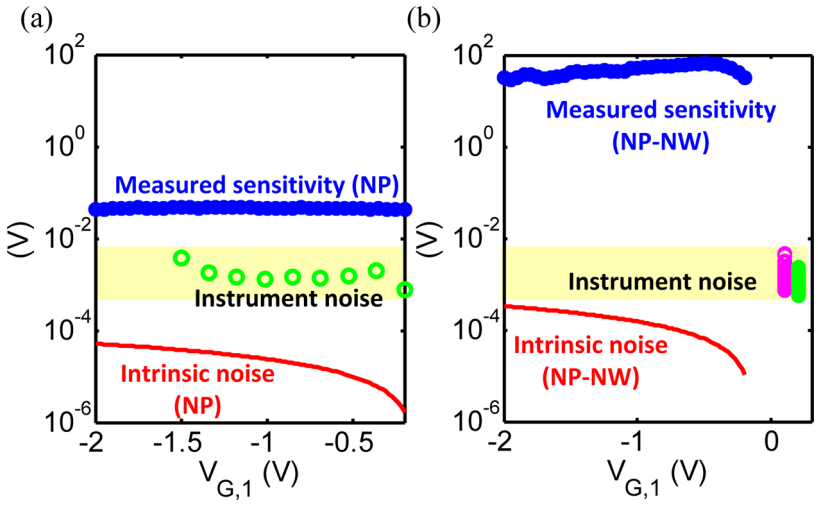

Figure 4. (a) Measured sensitivity (blue dots) of an isolated nanoplate (T_1) sensor and instrument noise (green circles) plotted as a function of nanoplate gate bias ($V_{G,1}$), as defined in Figure 1d. (b) Corresponding plot for the nanoplate−nanowire (T_1-T_2) sensor scheme proposed in this paper. The measured sensitivity in (b) represents the blue dots in Figure 2e. The theoretical lower limit of 1/*f* noise is also shown (red, solid curve). The details of theoretical noise limit can be found in the Supporting Information.

practical concerns of applying high bias on the gate oxide (for the bottom-gated NW corresponding to blue dots in Figure 2e) that may lead to leakage and hysteresis may also limit the maximum gain achievable from a NP−NW sensor combination.

Regarding the signal-to-noise ratio, another key parameter of pH sensors, it is important to realize that the *theoretical* lower limit of SNR and minimum pH resolution ($\Delta pH_{min} \equiv 3\delta V_G/S$ where δV_G is the gate voltage noise (V unit), and S is the pH sensitivity) of the GN scheme are still defined by those of its detector (T_1). In practice, however, fundamental considerations of measurement noise and biasing configuration ensure that the GN scheme achieves better ΔpH_{min} far more easily than either the NP or NW sensor could in isolation, as discussed below.

The 1/*f* noise is the dominant source of noise at frequencies relevant for pH sensors,[17] and its power spectral density is given by $S_{V_G} \approx \langle \delta V_G^2 \rangle \propto 1/A$ (A is the device area) or $(\langle \delta V_G^2 \rangle)^{1/2} \approx \gamma/\sqrt{A}$ (γ is a prefactor: see Sec. II in the Supporting Information). For a typical *single* NW pH sensor this noise floor limits the pH resolution to

$$\Delta pH_{min}^{NW} \sim 3\sqrt{\langle \delta V_{G,NW}^2 \rangle}/0.059 \sim 3\gamma_{NW}/(0.059\sqrt{A_{NW}}) \quad (5)$$

Indeed, a key concern for typical NW pH sensors is that such low resolution due to a small A_{NW} might be unacceptable for many physiological applications.[18]

On the other hand, if the larger area NP sensor (T_1) was used *in an ISFET configuration*, the noise floor (red solid line, Figure 4a) improves the pH resolution considerably, *i.e.*,

$$\Delta pH_{min}^{NP} \sim 3\sqrt{\langle \delta V_{G,NP}^2 \rangle}/0.059 \sim 3\gamma_{NP}/(0.059\sqrt{A_{NP}}) \quad (6)$$

as defined by the vertical gap (in log plot) between the blue dots and the red lines in Figure 4a. For the NP−NW sensor used in the GN scheme, pH sensitivity is amplified ($0.059 \times \alpha_{GN}$, blue dots in Figure 4b) and so is the voltage noise (red curve in Figure 4b). However, its pH resolution is still fundamentally limited by NP (T_1) noise because if an instantaneous pH signal is unresolved in the NP sensor due to noise, it will also remain unresolved in the NP−NW combination; thus $\Delta pH_{min}^{NP\text{-}NW} = \Delta pH_{min}^{NP}$. Nevertheless, since $A_{NP} \gg A_{NW}$, the pH resolution is considerably improved compared to the single NW sensor: this improvement reflects the reduction in noise floor due to the larger area of the NP sensor itself (T_1), not due to the NP−NW (T_1-T_2) combination.

The additional SNR advantage of the T_1-T_2 combination becomes apparent, however, when the noise of the measurement instrument, δV_{Ins}, is taken into account. If $\delta V_{NP} < \delta V_{Ins}$, as can always be conveniently arranged by increasing the size of the NP (T_1) transistor, we find that the pH resolution for the NP alone would have been limited by instrument noise, *i.e.*, $\Delta pH_{min}^{ins}|_{NP} \approx 3(\langle \delta V_{ins}^2 \rangle)^{1/2}/0.059 \gg \Delta pH_{min}^{NP}$, and therefore the signal from the NP alone will remain poorly resolved. However, the same signal can still be detected by the T_1-T_2 combination as $\Delta pH_{min}^{ins}|_{NP-NW} \approx 3(\langle \delta V_{ins}^2 \rangle)^{1/2}/(0.059\alpha_{GN})$ if δV_{ins} is larger than δV_{NW} and δV_{NP}; thus $\Delta pH_{min}^{ins}|_{NP} \gg \Delta pH_{min}^{ins}|_{NP-NW}$ (see Table S1 in the Supporting Information). This is illustrated by the increasing gap between instrument noise (yellow band) and sensitivity (blue dots) in Figure 4a *vs* b, respectively. This is because in the GN scheme the sensitivity is amplified by the area ratio, while the noise depends on the square root of the area. Note that this improvement cannot be obtained by simply adding an amplifier following a sensor node, because the SNR ratio remains unchanged in that case.

CONCLUSION

In this paper, we have established a theoretical framework of a new class of ISFET sensors that achieves high sensitivity by physically decoupling the sensor from the transducer node. This principle was used to design a nanoplate–nanowire transistor pair, which showed (consistent with theoretical prediction) sensitivity > 10 V/pH, which is significantly higher than previous reports based on DGFET pH sensors. Furthermore, we show that pH sensitivity close to 100 V/pH may *potentially* be achieved by incorporating high-mobility materials as a sensor node coupled to a low-mobility transducer. The high sensitivity improves the pH resolution as well as signal-to-noise ratio, especially when sensor precision is limited by the noise of the measurement instrument. The improvement of sensitivity, however, must be counterbalanced against the requirement of a dynamic range for pH sensing and practical requirements of device scaling. This generic nature of the concept, combined with its compatibility with conventional top-down CMOS processing technology, should make the concept relevant for applications in biomedical areas such as proton-based genome sequencers, environmental toxin monitoring, and pharmaceutical testing, in which precise pH monitoring is critical to its sequencing accuracy.

METHOD

Fabrication Process of Nanowire and Nanoplate Devices. The devices were fabricated using top-down fabrication, starting with bonded SOI wafers. Eight-inch bonded SOI wafers (SOITECH) p-type doped at 10^{15}/cm^2 with a box thickness of 145 nm and superficial silicon thickness of 55 nm were first laser cut into 4 in. wafers by Ultrasil Corp. The wafers were then oxidized for 11 min at 1000 °C to grow 30 nm of oxide and placed into buffered oxide etch (BOE) to thin down the top silicon to around 350 Å. Wafers were doped with boron at 10 keV at a dose of 10^{14} cm^{-2} and a tilt of 7°. Next, the gate dielectric was formed. For SiO_2 devices, the wafers were dry oxidized for 1 min at 1000 °C to form a gate oxide of around 50 Å, which was measured *via* ellipsometry on monitor wafers also present during the oxidation run. This also served as a dopant activation step. For HfO_2 devices, after a brief BOE dip and dopant activation in nitrogen for 3 min at 1000 °C, the wafers were placed into an atomic layer deposition machine for 150 cycles of HfO_2 for a target thickness of 150 Å. Wafers were then subjected to a rapid thermal anneal for 1 min at 950 °C, followed by a forming gas anneal for 30 min at 450 °C in 5% H_2 in N_2 to reduce interfacial trapped charges, mobile charges, and fixed charges. Next, channels were formed on the silicon surfaces with optical lithography and subsequent BOE etch to make solid, crack-free connections between metal interconnects and the silicon layers. AFM was performed over these regions to determine the silicon thickness (~300 Å) and the gate dielectric thickness (~50 Å for SiO_2, 150 Å for HfO_2).

Device Measurement in pH Environment. The pH measurements utilized two separate devices. The main sensing chip with the nanoplate device (2 μm wide) had a 150 Å thick HfO_2 dielectric, while the device exhibiting the GN response (a 50 nm wide nanowire device) contained a 50 Å thick SiO_2 dielectric. Both chips were fitted with open PDMS wells for containing the fluid. The pH values for each solution were measured separately with a commercial pH meter. The fluidic environments over the two separate chips were biased with two leak-free Ag/AgCl reference electrodes purchased from Warner Instruments. A 1× phosphate buffer saline solution at pH 7.4 was used for the nanowire device for the entire experiment to enable normal transfer characteristics. Robinson buffers (0.04 M phosphoric, boric, and acetic acid) with titrated HCl and NaOH, which have good buffering capacity over wide pH ranges, were manually pipetted and rinsed in the PDMS well over the nanoplate device, followed by a 5 min settling time to allow the surface charge to equilibrate. Transfer characteristics were measured using a Keithley 4200 semiconductor characterization system. The source and drain nodes of the devices were shorted together to create the full GN response sensor, and current was measured at the shorted source nodes of the devices.

Conflict of Interest: The authors declare no competing financial interest.

Acknowledgment. We acknowledge financial supports from National Institutes of Health (NIH, R01-CA20003), Materials, Structures and Devices (MSD) Focus Center, and computational resources from Network for Computational Nanotechnology (NCN).

Supporting Information Available: Detailed theoretical analysis regarding bias-dependent sensitivity; signal-to-noise ratio and pH resolution of giant-Nernst scheme. This material is available free of charge *via* the Internet at http://pubs.acs.org.

REFERENCES AND NOTES

1. Beckman, A. O.; Fracker, H. E. Apparatus for Testing Acidity, U.S. Patent 2,058,761, 1936.
2. Bergveld, P. Thirty Years of ISFETOLOGY: What Happened in the Past 30 Years and What May Happen in the Next 30 Years. *Sens. Actuators B: Chem.* **2003**, *88*, 1–20.
3. Patolsky, F.; Zheng, G.; Lieber, C. M. Nanowire-Based Biosensors. *Anal. Chem.* **2006**, *78*, 4260–4269.
4. Star, A.; Gabriel, J.-C. P.; Bradley, K.; Grüner, G. Electronic Detection of Specific Protein Binding Using Nanotube FET Devices. *Nano Lett.* **2003**, *3*, 459–463.
5. Rothberg, J. M.; Hinz, W.; Rearick, T. M.; Schultz, J.; Mileski, W.; Davey, M.; Leamon, J. H.; Johnson, K.; Milgrew, M. J.; Edwards, M.; *et al.* An Integrated Semiconductor Device Enabling Non-optical Genome Sequencing. *Nature* **2011**, *475*, 348–352.
6. Spijkman, M.-J.; Brondijk, J. J.; Geuns, T. C. T.; Smits, E. C. P.; Cramer, T.; Zerbetto, F.; Stoliar, P.; Biscarini, F.; Blom, P. W. M.; de Leeuw, D. M. Dual-Gate Organic Field-Effect Transistors as Potentiometric Sensors in Aqueous Solution. *Adv. Funct. Mater.* **2010**, *20*, 898–905.
7. Spijkman, M.; Smits, E. C. P.; Cillessen, J. F. M.; Biscarini, F.; Blom, P. W. M.; de Leeuw, D. M. Beyond the Nernst-Limit with Dual-Gate ZnO Ion-Sensitive Field-Effect Transistors. *Appl. Phys. Lett.* **2011**, *98*, 043502.
8. Knopfmacher, O.; Tarasov, A.; Fu, W.; Wipf, M.; Niesen, B.; Calame, M.; Schonenberger, C. Nernst Limit in Dual-Gated Si-Nanowire FET Sensors. *Nano Lett.* **2010**, *10*, 2268–2274.
9. Go, J.; Nair, P. R.; Reddy, B.; Dorvel, B.; Bashir, R.; Alam, M. A. Beating the Nernst Limit of 59 mV/pH with Double-Gated Nano-Scale Field-Effect Transistors and its Applications to Ultra-Sensitive DNA Biosensors. Electron Devices Meeting (IEDM), 2010 IEEE International.
10. Bousse, L.; De Rooij, N. F.; Bergveld, P. Operation of Chemically Sensitive Field-Effect Sensors as a Function of the Insulator-Electrolyte Interface. *IEEE Trans. Electron Devices* **1983**, *30*, 1263–1270.
11. Stern, E.; Klemic, J. F.; Routenberg, D. A.; Wyrembak, P. N.; Turner-Evans, D. B.; Hamilton, A. D.; LaVan, D. A.; Fahmy, T. M.; Reed, M. A. Label-Free Immunodetection with CMOS-Compatible Semiconducting Nanowires. *Nature* **2007**, *445*, 519–522.
12. Bard, A. J.; Faulkner, L. R. *Electrochemical Methods: Fundamentals and Applications*; John Wiley: New York, 1980.

13. Kokawa, T.; Sato, T.; Hasegawa, H.; Hashizume, T. Liquid-Phase Sensors Using Open-Gate AlGaN/GaN High Electron Mobility Transistor Structure. *J. Vac. Sci. Technol. B* **2006**, *24*, 1972–1976.
14. Steinhoff, G.; Hermann, M.; Schaff, W. J.; Eastman, L. F.; Stutzmann, M.; Eickhoff, M. pH Response of GaN Surfaces and its Application for pH-Sensitive Field-Effect Transistors. *Appl. Phys. Lett.* **2003**, *83*, 177.
15. Vu, X. T.; GhoshMoulick, R.; Eschermann, J. F.; Stockmann, R.; Offenhäusser, A.; Ingebrandt, S. Fabrication and Application of Silicon Nanowire Transistor Arrays for Biomolecular Detection. *Sens. Actuators B: Chem.* **2010**, *144*, 354–360.
16. Chen, S.; Bomer, J. G.; Carlen, E. T.; van den Berg, A. Al_2O_3/Silicon NanoISFET with Near Ideal Nernstian Response. *Nano Lett.* **2011**, *11*, 2334–2341.
17. Jakobson, C. G.; Nemirovsky, Y. 1/f Noise in Ion Sensitive Field Effect Transistors from Subthreshold to Saturation. *IEEE Trans. Electron Devices* **1999**, *46*, 259–261.
18. Zhang, X.; Ju, H.; Wang, J. *Electrochemical Sensors, Biosensors and their Biomedical Applications*; Academic Press: New York, 2007.